



Performance of Al-MCM-41 nanospheres as catalysts for dimethyl ether production

J.C. Bedoya ^{a,b}, R. Valdez ^b, L. Cota ^b, M.A. Alvarez-Amparán ^{a,b}, A. Olivas ^{b,*}

^a Centro de Investigación Científica y de Educación Superior de Ensenada (CICESE), km. 107 Carretera Tijuana-Ensenada, Apdo. Postal 14, CP. 22800, Ensenada, BC, Mexico

^b Centro de Nanociencias y Nanotecnología (CNyN-UNAM), Universidad Nacional Autónoma de México, km. 107 Carretera Tijuana-Ensenada, Apdo. Postal 14, CP. 22800, Ensenada, BC, Mexico

ARTICLE INFO

Keywords:

DME
Methanol-dehydration
Al-MCM-41-nanospheres
Alternative fuels
Nanocatalysts materials

ABSTRACT

The need to develop specific-morphology nanomaterials to produce dimethyl ether (DME), a promissory alternative fuel, by the catalytic methanol dehydration has triggered extensive research to synthesize novel materials. In this work mesoporous Al-MCM-41 nanospheres with variable size (35–90 nm) were synthesized by the *sol-gel* method. The size of the Al-MCM-41 nanospheres was controlled by adjustable NaOH/TEOS ratio (0.2–0.5). The Al-MCM-41 nanospheres were characterized by TPD, TEM, XRD, EDX, XPS and N₂-physisorption. According to the characterization results the Al ions were successfully incorporated in the MCM-41 framework and the Al-MCM-41 nanospheres showed hexagonal and mesoporous structure. Additionally, it was observed that the higher the NaOH/TEOS ratio the smaller size of the nanosphere and, smaller Al-MCM-41 nanospheres presented more amount of medium acidic sites on its surface. The catalytic activity results showed that all samples tested reached 100% of selectivity towards DME. The smallest Al-MCM-41 nanospheres achieved 78% of DME yield at 300 °C and good catalytic activity performance below to 300 °C. The stability of the fresh and regenerated Al-MCM-41 nanospheres was evaluated for 48 h time-on-stream. High values of DME yield (> 60%) were maintained during 48 h time-on-stream showing the possibility for recycling the material.

1. Introduction

Dimethyl ether (DME) has gained significant attention for replacing diesel fuel and LPG (liquid petroleum gas) because of its similar physicochemical properties and thermal efficiency [1,2]. DME is considered as a green fuel since its combustion produces low NO_x emissions, zero SO_x emissions, and negligible smog amounts. Also, DME could be used as chemical intermediate for obtaining high added-value chemicals such as lower olefins, methyl acetate, and dimethyl sulphate [3]. Although DME is a volatile compound, it is not toxic, nor carcinogenic, or mutagenic for humans, and it is environmentally friendly [1–4]. DME could be stored in a gas phase under ambient conditions or in a liquid phase at high pressure (~0.5 MPa at 25 °C). Therefore, DME could be easily handled and transported using the current LPG technology [5].

Nowadays, DME can be produced through two-step or one-step processes. In the first one, methanol is obtained from CO and H₂ as intermediate compound commonly using copper-based catalysts, later DME is obtained by methanol dehydration using acid solids as catalysts.

Also, bifunctional catalysts have been proposed to be used in the two-step process to produce simultaneously methanol and DME. In the one-step process crude methanol is dehydrated to obtain DME using acidic solids as catalysts, usually Al₂O₃-based materials. Methanol dehydration over acidic-solid materials produce dimethyl ether and water as reaction products in a reversible process (2CH₃OH ↔ CH₃OCH₃ + H₂O). Fig. 1 shows the chemical routes to produce DME in two-step or one-step processes [2].

Methanol dehydration usually is carried out using γ-Al₂O₃ [6–9] or zeolites [10–13] as catalysts. γ-Al₂O₃ is used due to its great specific surface area, uniform pore size distribution, high thermal resistance and high DME selectivity. However, this material presents weak surface acidity and therefore presents low catalytic activities [2]. Zeolites are commonly employed in this reaction due to the presence of acid sites, as well as high hydrothermal stability and suitable reactivity at low temperatures. Nevertheless, zeolites generate by-products such as coke and low-molecular weight hydrocarbons, which reduce DME selectivity and catalyst life [2].

* Corresponding author.

E-mail address: aolivas@cnyt.unam.mx (A. Olivas).

Ordered mesoporous materials present outstanding properties as tunable surface areas, large pore sizes (2–50 nm), and well-ordered framework. In particular, pure siliceous MCM-41 exhibits an ordered hexagonal mesoporous assembly, high specific surface areas (800–1200 m²/g) and average pore size of ~2 nm [14]. These features of MCM-41-based materials promotes a suitable diffusion of reactants and products in catalytic reactions.

The pristine MCM-41 material does not have significant acidity. However, surface acidic sites can be incorporated by replacing silicon atoms of the MCM-41 framework with metallic atoms such as Al [15], Fe [16], Ga [17], Zr [18] and Sn [19]. Also, the acidity strength, type of acidity, and quantity of acid sites can be controlled by the amount and dispersion of metallic atoms over silica framework [20]. Silicon atoms in the silica structure can be replaced by post- and direct-synthesis. In the former, the quantity of surface acidic sites is relatively low, and heteroatoms are kept on the surface by electrostatic forces, which could be quickly leached out in the reaction [21,22]. The direct synthesis involves an isomorphic substitution that embeds the metallic heteroatoms into the framework with high dispersion and allows acidity control [23]. Moreover, metallic heteroatoms are attached to silicon through a covalent Si-O-M bridge, reducing their leaching in the reaction [24].

Doped MCM-41 materials have been used in many reactions of interest. For example, MCM-41 and modified MCM-41 materials have been used as catalytic materials for pollutant degradation [25], CO₂ capture [26], oxidation of o-xylene [27], biomass pyrolysis processes [28], photocatalytic process as water splitting [29], hydrodesulfurization of refractory compounds [30], DME production [31] and several other catalytic applications [23].

In a recent study, Sang et al., stated that M-MCM-41 (M = Al, Fe, Ga, Zr, and Sn) materials presented different surface acidity according to the coordination of the metallic ion added as well as to the amount of dopant ion. Also, it was found that Al-MCM-41 with a Si/Al molar ratio of 5 and 10 were the most active catalysts in the methanol dehydration to obtain DME at high temperatures (300–450 °C) [32]. Naik et al., also have shown the catalytic performance of Al-MCM-41 materials, with high Si/Al molar ratio and different synthesis methods, for DME production by the methanol dehydration reaction [33].

The morphology and size of bulk MCM-41 could be modified to the nanoscale, providing new materials with unique physicochemical and catalytic properties. For example, Yu Chen et al., synthesized spherical MCM-41 nanoparticles of several diameters in the range of 40–160 nm, by adjusting the sol-gel synthesis conditions [34].

In this paper, to deepen and expand knowledge about new Al-MCM-41 materials applied to the production of DME as well as to elucidate in correct way the effect of the Al-MCM-41 nanoparticles with different size, we synthesized Al-MCM-41 nanospheres (5 < Si/Al molar ratio < 7) controlling the diameter of the nanospheres through of the modification of the typical sol-gel method. Additionally, the textural and structural properties of the modified Al-MCM-41 materials was related with the catalytic properties of the material in the methanol dehydration to produce DME.

2. Experimental

2.1. Controlled synthesis of Al-MCM-41 nanospheres

Al-MCM-41 nanospheres were synthesized by the sol-gel method proposed by Chen et al., [34]. A solution (A) was prepared by dissolving 0.223 g of aluminum isopropoxide (Aldrich, 98%) in 40 mL of ethanol during 5 min in ultrasonic bath and later the solution was stirred at 25 °C for 1 h. Afterward, 2.43 mL of TEOS (Aldrich, 98%) was added to the solution and was stirred at 300 rpm for 15 min. A Si/Al molar ratio in the 5–7 range was maintained in all materials. Another solution (B) was prepared by mixing 192 mL of distilled water with 1.4 mL of NaOH 2 M and 0.4 g of CTAB (Aldrich, 98%). Solution B was stirred at 300 rpm at 80 °C in a reflux system. Subsequently, the solution (A) was added dropwise to the solution (B), the resulting mixture was stirred at 300 rpm at 80 °C for 2 h. The obtained sol-gel had a molar composition of 119H₂O:0.3NaOH:0.125CTAB:0.1Al(O-i-Pr)₃:1TEOS. The sample was centrifuged and rinsed with distilled water until a neutral pH value was obtained and later was dried at 100 °C for 12 h. Finally, the dried samples were calcined at 600 °C for 5 h in air using a conventional muffle furnace at a heating rate of 3 °C/min. Also, Al-MCM-41 nanoparticles of different diameters was prepared by varying the molar ratio of NaOH/TEOS in a range from 0.2 to 0.5. The samples were labeled according to the NaOH/TEOS ratio as Al-MCM-41_x, where "x" correspond to the NaOH/TEOS ratio as is shown in Table 1.

2.2. Characterization of materials

Low-angle X-ray diffraction patterns were recorded in a Philips X'Pert diffractometer in the 2θ range from 1.5° to 8°, using CuK_α radiation ($\lambda = 1.5406 \text{ \AA}$) at 45 kV and 30 mA. The morphology of the materials was observed by a JEOL JEM-2010 transmission electron microscope (TEM) operating at 200 kV. Textural properties were determined from the adsorption-desorption of N₂ isotherms using a

Table 1
Chemical composition and textural properties of the Al-MCM-41_x nanospheres.

Material	NaOH/ TEOS	D _s ^a (nm)	S _{BET} ^b (m ² / g)	D _p ^c (nm)	V _p ^d (cm ³ / g)	Si	Al	Si/ Al
Atomic %								
Al-MCM-41_0.2	0.2	35	1137	2.22	1.03	20.1	2.8	7.1
Al-MCM-41_0.3	0.3	45	1083	2.06	0.78	21.7	3.2	6.9
Al-MCM-41_0.4	0.4	60	1066	2.03	0.46	21.8	4.6	4.7
Al-MCM-41_0.5	0.5	90	837	2.12	0.55	20.7	3.7	5.7

^a Average sphere diameter.

^b Brunauer-Emmett-Teller surface area.

^c Average pore diameter.

^d Cumulative pore volume.

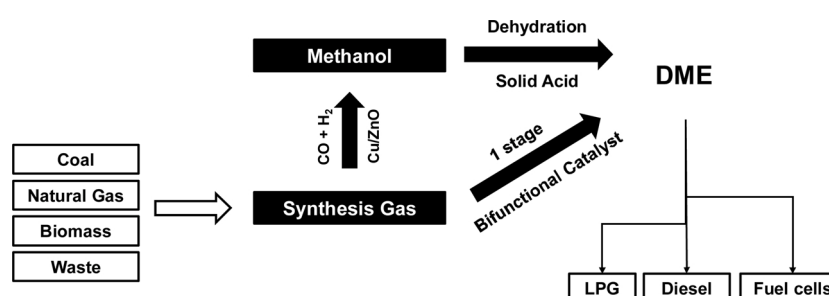


Fig. 1. Scheme of the several routes for the synthesis of dimethyl ether.

Micromeritics Tristar II apparatus at -196°C . The materials were degassed at 200°C for 4 h before the physisorption measurements. The specific surface area was determined from 0.05 to 0.25 as relative pressure (P/P_0) using the Brunauer-Emmett-Teller (BET) equation. Cumulative volume and average pore sizes were determined using the BJH method in the desorption branch. Energy dispersive X-ray spectroscopy (EDX) was performed in a Zeiss MA EVO-15 scanning electron microscope (SEM) to estimate the elemental composition of the materials. The surface acidity was determined by recording the temperature-programmed desorption ($\text{NH}_3\text{-TPD}$) profile of the samples using a ChemBET Pulsar TPR/TPD equipment. A mass catalyst of 53 mg was used for the ammonia TPD measurements. Initially, physisorbed water and organic molecules were removed from the catalytic surface using a helium flow (120 mL/min) from room temperature up to 550°C at a heating rate of $10^{\circ}\text{C}/\text{min}$. After cooling the sample up to 50°C , high purity NH_3 flow (120 mL/min) was passed through the sample for 10 min at 50°C . The excess of NH_3 was removed at 50°C under a helium atmosphere during 40 min. Finally, TPD profiles were recorded from 50 to 550°C using helium as gas carrier.

The surface chemical composition was determined by X-ray photoelectron spectroscopy (XPS) using a SPECS PHI-548 equipment with an aluminum anode ($\text{K}\alpha = 1486.6 \text{ eV}$, 300 W). XPS measurements were calibrated by fixing the C 1s peak of the adventitious carbon at 284.5 eV.

2.3. Catalytic activity

The Al-MCM-41 nanospheres were tested in the catalytic methanol dehydration to produce DME. The catalytic tests were carried out in a tubular stainless steel fixed-bed reactor from 100 to 400°C and atmospheric pressure. Before a typical catalytic test, the sample (0.2 g) were pretreated at 450°C with N_2 flow (20 mL/min) for 1 h to remove physisorbed water. Afterwards, methanol (0.33 mL/h) was fed to the reactor using a mass flow controller and nitrogen as carrier gas (20 mL/min), the space velocity (WHSV) was 7.5 h^{-1} . The reaction products were analyzed four times at intervals of 30 min, at the desired temperature, using an online HP 6890 Series I gas chromatograph equipped with a thermal conductivity detector and Supelcowax-10 (Bonded; polyethylene glycol) fused silica capillary column (30 m length, 0.53 mm I.D., and 0.5 μm film thickness). To avoid the condensation of the reaction products, the output gas lines of the reactor were maintained at 150°C . The selectivity towards DME was 100% in the catalytic methanol dehydration reaction according to the chromatographic analysis results, for all catalytic tests.

3. Results and discussion

Low-angle XRD patterns of the Al-MCM-41_x nanospheres are shown in Fig. 2. The peak at 2.3° was assigned to the diffraction of the plane (100) of an ordered 2d-hexagonal array (p6mm) associated to the mesoporous MCM-41 structure (ICDD # 49-1712). The broad and low-intensity diffraction peak in the samples was attributed to a well-defined structure with small dimensions. In this sense, Kosslick et al., has established the shrinkage of the hexagonal array of MCM-41 materials by the aluminum incorporation [35], as well as it has been established the same observation in several published works [15–19,23]. According to Sang et al., the broadening of the (100) diffraction is attributed to a change of the bond angle of the Al-O-Si due to Al ion incorporation, compared to the bond angle of Si-O-Si matrix [32]. The absence of (110) and (200) diffractions of Al-MCM-41_x nanospheres could suggest confirmation of change of the bond angle of Al-O-Si. Also, it is interestingly to note, according to the XRD results, that different NaOH/TEOS ratios do not modify the hexagonal structure of the nanospheres.

Fig. 3 shows the TEM micrographs of the Al-MCM-41_x nanospheres. The samples displayed similar morphology consisting of spherical-like nanoparticles of high porosity. The porous structure typical of MCM-41-based materials is observed for all samples. The Al-MCM-41_x

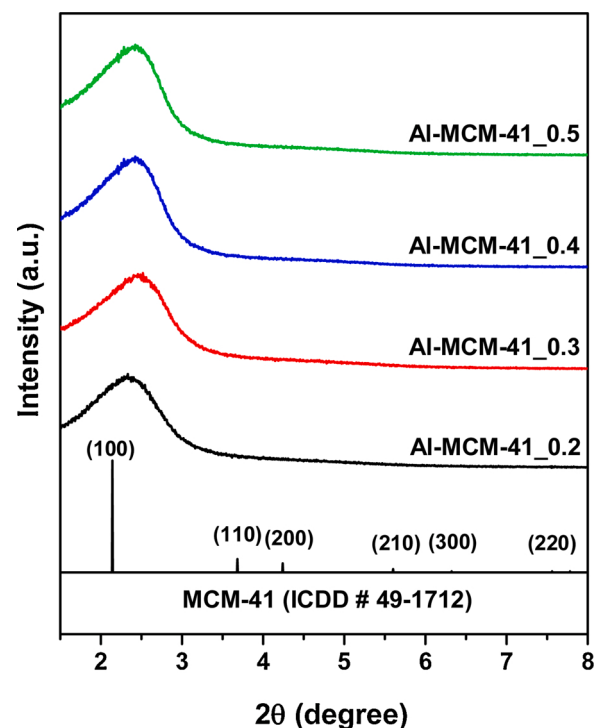


Fig. 2. Low-angle X-ray diffraction patterns of the Al-MCM-41_x samples.

nanostructures presented different size in function of the NaOH/TEOS ratio (see Fig. 3 and Table 1). The nanoparticles size ranges from 35 to 90 nm for different NaOH/TEOS ratios (0.2–0.5). The higher the NaOH/TEOS ratio, the larger the size of the nanoparticles. The greatest effect of the NaOH/TEOS ratio on the nanoparticles size is observed with higher NaOH/TEOS ratio (0.4 or 0.5) because the increase in the nanoparticles size is greater when NaOH/TEOS ratio goes from 0.4 to 0.5, compared when NaOH/TEOS ratio goes from 0.2 to 0.3. This result is due to the generation of larger micelles during the formation process of the sol.

The sample synthesized using the lowest NaOH/TEOS ratio (Al-MCM-41_0.2) exhibited spherical-like nanoparticles with straight edges, as shown in Fig. 3(a). The presence of straight edges is explained by the sol-gel synthesis mechanism proposed by Yu et al., [34] where the assembly of hexagonal aligned micelles leads to the formation of spherical-like nanoparticles of MCM-41. For the Al-MCM-41_x samples, the spherical-like morphology of the nanoparticles remained without changes after the aluminum incorporation.

The elemental analysis by EDX is shown in Table 1. The experimental Si/Al molar ratio was in the range of 5–7. According to previous reports, the Al-MCM-41 samples with Si/Al molar ratio of 5 or 10 showed enhanced catalytic and textural characteristics compared with samples with Si/Al molar ratio greater than 10 [32–34]. Therefore, the size of the Al-MCM-41 nanospheres was function of the amount of NaOH in the synthesis process, as was stated by Chen et al. [34]. The N_2 adsorption/desorption isotherms of the Al-MCM-41 nanospheres are shown in Fig. 4a. The Al-MCM-41 nanospheres showed type IV isotherms which confirm the presence of cylindrical mesoporous typical of MCM-41 materials. The formation of a monolayer occurs at low relative pressures <0.05 . The formation of multilayers occurs subsequently undergo a phenomenon of capillary condensation on the adsorbent surface as is shown from 0.05 to 0.3 (P/P_0). The H3 hysteresis loop (0.9–1.0 P/P_0) suggest the presence of large mesopores and also, that adsorption and desorption follow the similar path which results in more efficient mass transfer phenomena, which favors the catalytic reactions. Table 1 summarizes the texture properties, specific surface area, cumulative pore volume and average pore diameter. It can be observed that surface

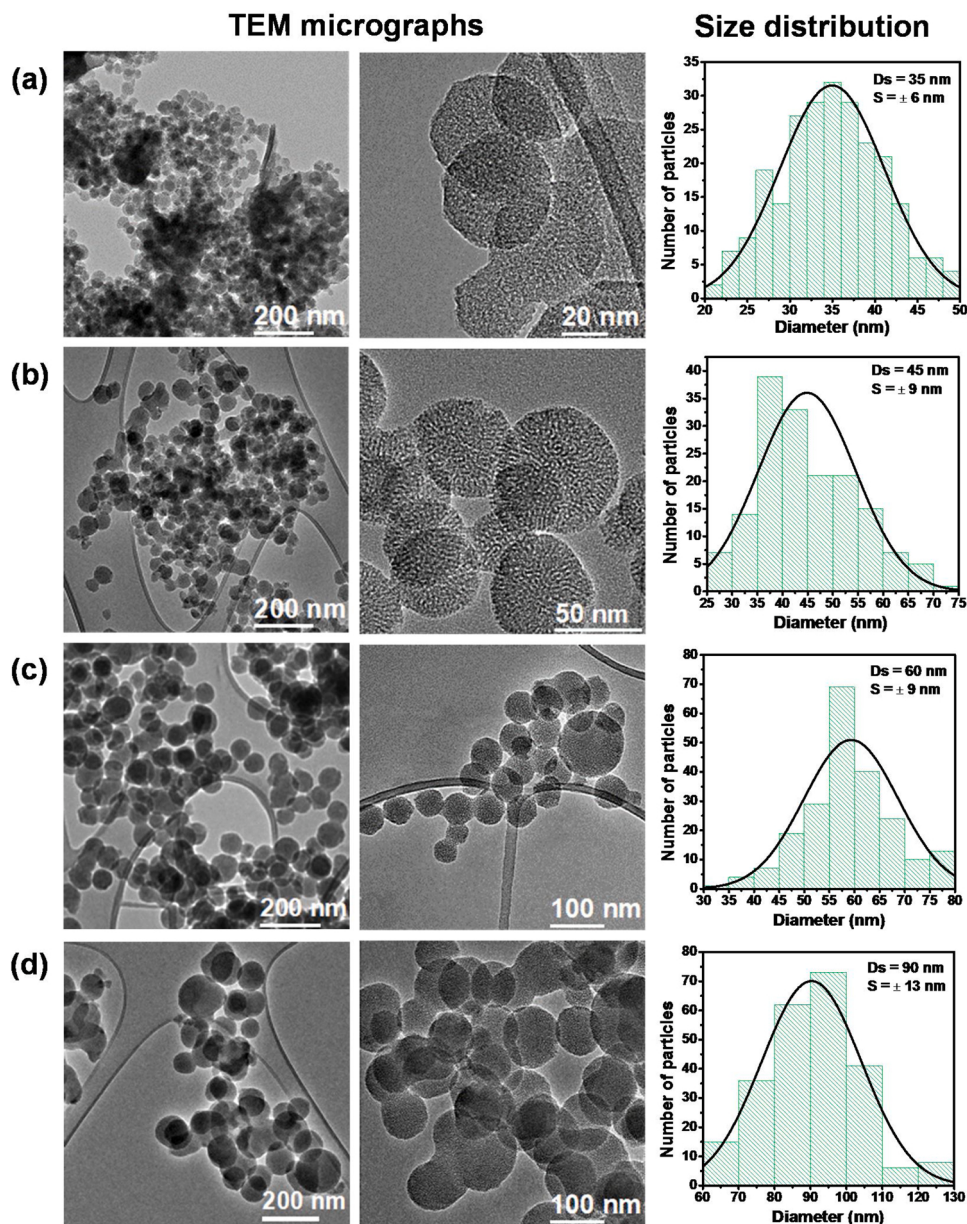


Fig. 3. Bright-field TEM micrographs of the catalyst; a) Al-MCM-41_0.2, b) Al-MCM-41_0.3, c) Al-MCM-41_0.4, and d) Al-MCM-41_0.5.

area is lower when the quantity of NaOH is high (high NaOH/TEOS ratio). The Al-MCM-41_x nanospheres with NaOH/TEOS ratio of 0.2 and 0.5 had surface areas of 1137 and 837 m²/g, respectively. Probably, at higher NaOH content some internal walls could be partially blocked, and simultaneously new pores be generated on the surface, which would decrease the surface area compared to the lower NaOH/TEOS ratio in Al-MCM-41_x nanospheres. Similarly, the pore volume values diminish according the NaOH content, in a similar trend as surface area, due to the minor intraparticle void. The average pore diameter was similar in all samples (~2 nm) due to the similar size of Al and Si ions therefore, the isomorphic substitution has very little influence on this parameter.

Fig. 4b shows the relationship between the surface area and the diameter of the nanospheres. As it can be observed the surface area was inversely proportional to the nanosphere size. That is, the larger the surface area the smaller the diameter of the nanospheres, a typical characteristic of nanomaterials. However, it is important to note that the surface area diminish in important extent when the NaOH content was maximum. These results could suggest that NaOH incorporation, in lower contents, slightly modify the initial framework of MCM-41 and did

not promote substantial changes of the textural properties of the original matrix, for example Al-MCM-41_0.2 presented the highest surface area value. Nonetheless, highest NaOH content (NaOH/TEOS = 0.5) could greatly distort the original matrix and abruptly modify the textural values, as it can be suggested by the lowest surface area value of Al-MCM-41_0.5.

NH₃-TPD analysis was made to determine the acidity and acidic strength of the active sites of the Al-MCM-41_x nanospheres. It is widely established that NH₃-desorption peaks at the intervals of 100–250, 250–400 and > 400 °C correspond to the weak-, medium-, and strong-strength acidic sites, respectively [36]. Usually, the NH₃-TPD profile for aluminosilicates materials shows desorption peaks corresponding to weak and medium acidic sites. The weak acidic centers are associated to ammonia physisorption meanwhile the medium acidic centers are assigned to strongly acidic silanol groups (Si – OH) [37]. The NH₃-TPD profiles of all Al-MCM-41_x nanospheres were deconvoluted using the included software of the ChemBET Pulsar TPR/TPD equipment. Fig. 5 shows the NH₃-TPD profile correspond to Al-MCM-41_0.2 nanospheres. In general, for all samples, two peaks were located between 100 and

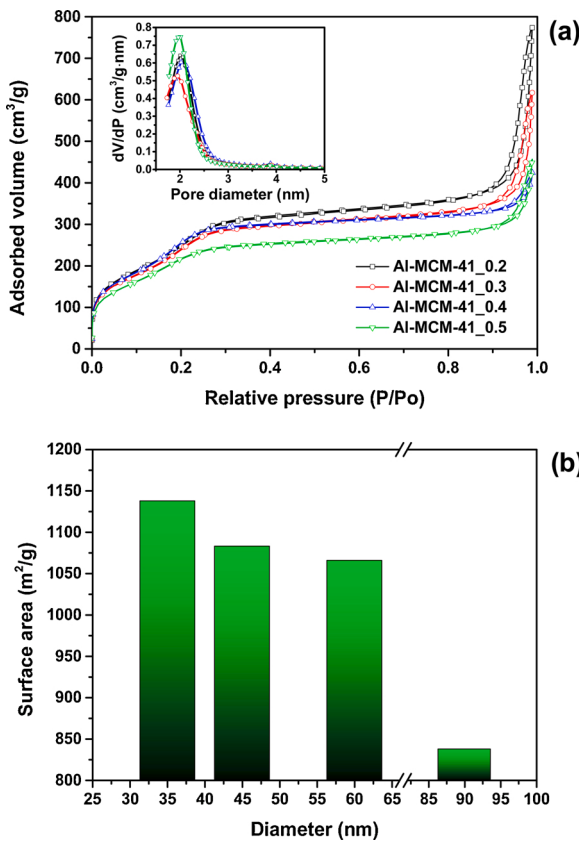


Fig. 4. a) N₂ adsorption-desorption isotherms for Al-MCM-41_x samples. b) Surface area versus the nanospheres diameter.

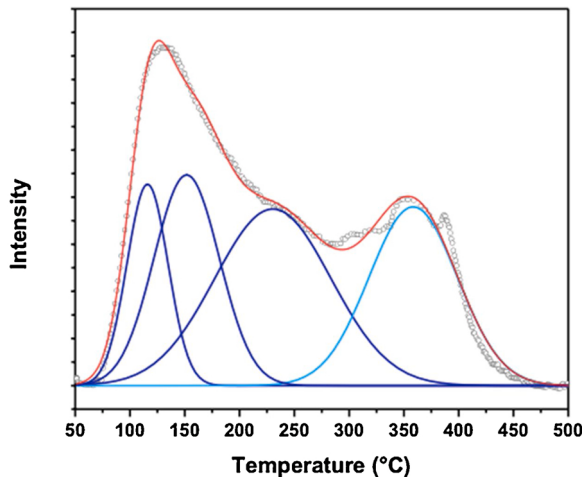


Fig. 5. TPD-NH₃ curve for the fresh Al-MCM-41_0.2 catalyst.

200 °C and were attributed to the presence of weak surface acidic sites. The widely overlapped desorption peak between 200 and 300 °C is associated with Lewis and Brønsted sites of weak acidic strength. The desorption peak centered at 370 °C is due to the medium acidic sites [38].

Table 2 shows the quantitative NH₃-TPD results for all Al-MCM-41_x nanospheres. As it can be observed the acidity was reported as total acidity, the amount of weak and medium acidic sites ($\mu\text{mol NH}_3/\text{g}_{\text{cat}}$) also was showed. According to the quantitative NH₃-TPD results show in Table 2, it is important to note that low acidic sites increased when NaOH/TEOS ratio was higher. That is, the higher NaOH content the

Table 2
Quantitative NH₃-TPD results of the Al-MCM-41_x samples.

Material	Acid site distribution ($\mu\text{mol NH}_3/\text{g}_{\text{cat}}$)			^a M _{ac} amount(%)
	Weak	Medium	Total	
Al-MCM-41_0.2	94.1	32.2	126.3	26
Al-MCM-41_0.3	140.4	36.3	176.7	21
Al-MCM-41_0.4	163.1	38.7	201.8	19
Al-MCM-41_0.5	179.1	21.3	200.4	11

* Medium acidic sites normalized to the corresponding total acidity.

more amount of low acidic sites. It can be observed that Al-MCM-41_0.5 nanospheres had the more amount of low acidic sites, contrary to what happens with Al-MCM-41_0.2 nanospheres. The nanospheres with NaOH/TEOS ratios of 0.2 and 0.3 had similar amount of medium acidic sites, opposite situation to Al-MCM-41_0.5, which could suggest that lower NaOH amount promotes the generation of medium acidic sites. The amount of medium acidic sites (% M_{ac}) indicated the greater amount of medium acidic sites for the Al-MCM-41 samples with lower NaOH content (lower NaOH/TEOS ratio), confirming the previously analysis. It has been documented that the catalytic activity in the methanol dehydration reaction was enhanced by the presence of medium acidic sites [39,40]. In this sense, it could be suggested that low NaOH content together Al³⁺ ions incorporation into MCM-41 matrix were favorable to increase the total surface acidity (Brønsted sites) and therefore could improve the catalytic methanol dehydration as it has been established in several studies using other catalytic materials [41].

The X-ray photoelectron spectroscopy (XPS) spectra of Al-MCM-41_0.2 is presented in Fig. 6. The general survey for all samples showed the presence of O (O 1s), Si (Si 2s, Si 2p), Al (Al 2p) y C (C 1s). The corresponding band at 284.5 eV was due to the presence of C used as signal for calibration. It can be observed, the bands of Si, O and Al which are characteristic of silicoaluminates materials. The deconvolution of Si 2p generates two bands at binding energies of 104.26 and 102.45 eV, respectively. The first one at 104.26 eV was assigned to Si⁴⁺ species, suggesting than amorphous SiO₂ was the main phase of the nanospheres. The shoulder at 102.45 eV was associated to the Si-O-Al bond. It is important to note that Si-O-Al binding energy was lower than Si-O-Si binding energy due to Al ions are less electronegative than Si ions [42, 43].

The catalytic performance of the Al-MCM-41 nanospheres, as a function of temperature, in the methanol dehydration reaction is shown in Fig. 7. It can be observed, for all samples, the higher temperature the higher the methanol conversion value and therefore the higher DME yield value (~99% of selectivity), in the range of temperatures of the catalytic tests (100–400 °C). The yield values at temperatures below of 200 °C were insignificant meanwhile the yield values at temperatures above of 300 °C were close to the equilibrium yield value. It is important to note that DME yield increased rapidly in the interval of 200–300 °C, unlike increasing DME yield at 100–200 °C and 300–400 °C temperature intervals. That is, although the maximum yield value of ~ 90% was reached from 350 °C and was constant to higher temperatures, the catalytic activity was considerably modified by the increase of temperature in the 200–300 °C interval. The inset in the Fig. 7 shows the DME yield versus temperature, from 230 to 270 °C. It can be observed that DME yield increased when the nanospheres diameter decreased. For example, at 250 °C, the DME yield using Al-MCM-41_0.2 (35 nm diameter) was 35% and this one was 3% higher than the DME yield using Al-MCM-41_0.3 (~32%) with 90 nm diameter. Meanwhile, the DME yield of Al-MCM-41_0.4 (60 nm diameter) and Al-MCM-41_0.5 (90 nm diameter) were similar (~29%). However, the higher catalytic activity at smaller diameter nanospheres is more evident at the 200–300 °C interval. At temperature intervals of 100–200 °C and 300–400 °C can be observed similar DME yield for bigger diameter nanospheres and a slightly higher DME yield for smaller diameter nanospheres. Also. It is important to note that the smaller nanospheres

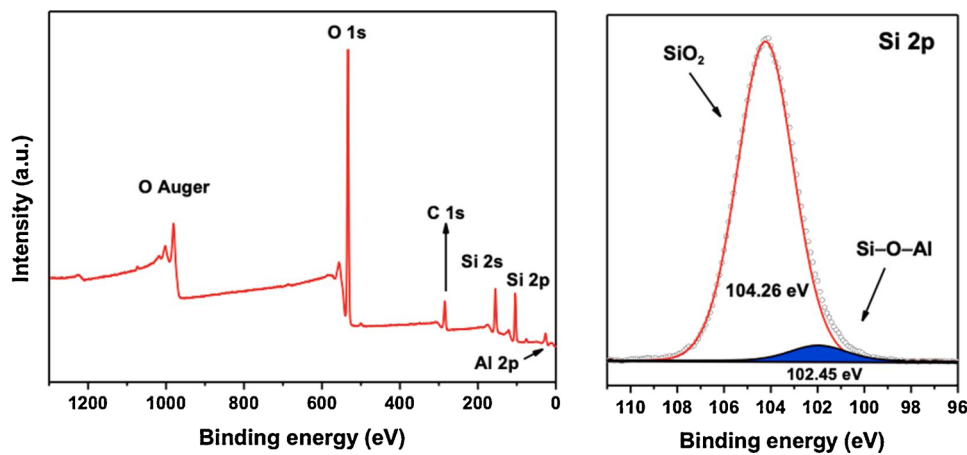
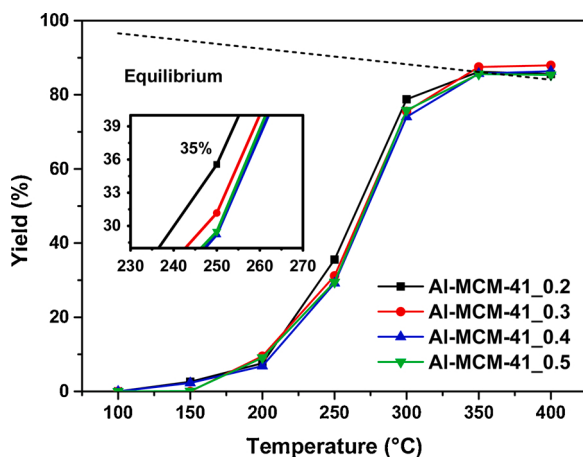


Fig. 6. XPS spectra for the fresh Al-MCM-41_0.2 nanospheres.

Fig. 7. DME yield using Al-MCM-41_x nanospheres as catalysts in the methanol dehydration.

presented more quantity of surface medium acidic sites, according to results showed in Table 2. Based on these results could be stated that smaller diameter nanospheres promoted the methanol dehydration and therefore the dimethyl ether production in all range of tested temperatures (100–400 °C). Therefore, the catalytic activity trend of the Al-MCM-41 nanospheres could be established as follow: Al-MCM-41_0.2 > Al-MCM-41_0.3 > Al-MCM-41_0.4 > Al-MCM-41_0.5. The greatest DME yield of ~90%, from 350 to 400 °C, was reached for all samples, however the DME yield was slightly greater for smaller diameter nanospheres. The DME yield values for Al-MCM-41_0.2 nanospheres, the smaller diameter nanospheres, at 200 and 300 °C were 35 and 78%, respectively. Therefore, it is important to note that high DME yield values are reached at temperatures below to 300 °C, according to the data trend showed in Fig. 7. The conversion and therefore the DME yield values reached by Al-MCM-41 nanospheres in this work were higher than methanol conversion values reported in published literature using solid materials in similar temperature ranges [32,44,45]. Additionally, it is important to note that dimethyl ether was the only reaction product obtained in the catalytic activity test (~99% of selectivity). Then, Al-MCM-41 nanospheres used as catalysts to methanol dehydration enhance the methanol conversion at temperatures below to 300 °C and improve the selectivity towards dimethyl ether (~99% of selectivity). The higher catalytic activity of the smaller diameter nanospheres could be attributed at i) the higher surface area, ii) higher surface-to-volume ratio (reaction occurs mostly at the surface), iii) shorter diffusion paths for smaller particles, leading to a more efficient mass transfer

process inside the nanospheres and iii) the more quantity of surface medium acidic sites.

The most active catalyst, Al-MCM-41_0.2, was used to determine the catalytic stability. The catalytic stability tests were determined at 300 °C. Firstly, Al-MCM-41_0.2 nanospheres were used in a typical catalytic reaction for 48 h time-on-stream. The initial DME yield with fresh Al-MCM-41_0.2 nanospheres was 78% (see Fig. 8) and decrease at 62% after 48 h time-on-stream. Therefore, DME yield of the Al-MCM-41_0.2 nanospheres diminish 16% during 48 h time-on-stream. Afterwards, the used sample was subjected to a regeneration process in a conventional muffle air at 600 °C for 5 h at a heating rate of 3 °C/min. The stability of the regenerated sample was also evaluated during 48 h time-on-stream. The initial DME yield of the regenerated Al-MCM-41_0.2 nanospheres was 68% and after 48 h time-on-stream decreases at 40%. That is, the DME yield of the regenerated Al-MCM-41_0.2 nanospheres falls 28% during 48 h time-on-stream.

It is important to note that the initial DME yield of the fresh Al-MCM-41_0.2 nanospheres was 10% greater than the initial DME yield of the regenerated Al-MCM-41_0.2 nanospheres. During 48 h time-on-stream, the DME yield falling of the fresh Al-MCM-41_0.2 nanospheres was 16% meanwhile the DME yield falling of the regenerated Al-MCM-41_0.2 nanospheres was 28%. Based on the above results can be observed that the stability of the fresh Al-MCM-41_0.2 nanospheres was greater than the stability of the regenerated Al-MCM-41_0.2 nanospheres. The lower catalytic activity and stability of the regenerated Al-MCM-41_0.2 nanospheres, respect to the fresh Al-MCM-41_0.2 nanospheres, could be explained due to the adsorption of surface carbon

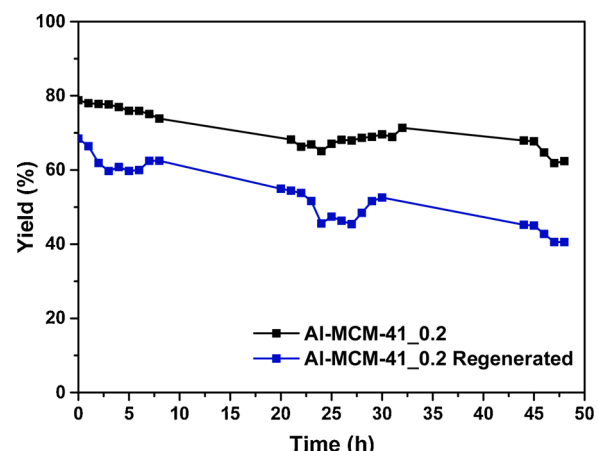


Fig. 8. DME-yield stability of the Al-MCM-41_0.2 nanospheres during 48 h time-on-stream in the methanol dehydration.

species (coke) during the methanol dehydration reaction. The Fig. 9 shows the TEM micrographs of the Al-MCM-41_0.2 nanospheres after 48 h of reaction. It can be observed that semi-spherical shape of the samples was conserved after 48 h of reaction however the edge of the nanospheres looked deformed. The black dots were due to coke over the surface. The adsorbed surface carbon species could hinder the internal-transport and adsorption of reagents (methanol and H₂) delaying the catalytic reaction and the later internal-transport and desorption of the products (H₂O and DME). Also, the presence of surface carbon species at high temperature (300 °C) could promote the sintering or agglomeration of the superficial Al or Si ions modifying the surface acidic. The above suggestions could explain the lower catalytic activity of the regenerated Al-MCM-41_0.2 nanospheres even immediately after the regeneration process.

The Table 3 shows a comparison of several typical mesoporous materials and the Al-MCM-41_0.2 nanospheres used in the catalytic methanol dehydration. The comparison was according to the catalyst load, the operating temperature and pressure. Al-MCM-41_0.2 nanospheres showed similar performance than other structures such as zeolites and alumina at the same operating conditions however Al-MCM-41_0.2 nanospheres loading used was lower than other catalysts. In other hand, the performance for Al-MCM-41_0.2 nanospheres is better than the bulk material at the same operation conditions [32]. The catalytic stability of Al-MCM-41_0.2 nanospheres in this work was monitored during 48 h time-on-stream and the decay of the catalytic activity (16%) could be mainly associated to the carbonaceous species adsorbed over the surface, see to Fig. 9. Additionally, the catalytic activity results of the reused Al-MCM-41_0.2 nanospheres after regeneration process,

indicating the possibility of reuse this material in several cycles.

4. Conclusions

Al-MCM-41 nanospheres with variable diameter was synthesized by the *sol-gel* method using CTAB as a template, NaOH for pH controlling and TEOS and aluminum isopropoxide as the aluminum and silicon source, respectively. To a constant Si/Al ratio the NaOH (as NaOH/TEOS ratios) was used to adjust the size of the Al-MCM-41 nanospheres. The smaller Al-MCM-41 nanospheres, synthesized at lower NaOH/TEOS ratios, presented 78% of dimethyl ether (DME) yield in the methanol dehydration reaction at 300 °C. The high catalytic activity was explained by the mesoporous and ordered-hexagonal structure that could enhance the diffusion of the reactants and products and, by the higher surface area and pore volume that could increase the amount of exposed active sites of medium acidity that promote the methanol dehydration. The catalytic activity of fresh and regenerated Al-MCM-41 nanospheres during 48 h time-on-stream was maintained with low DME-yield falling (16%) for the fresh Al-MCM-41 nanospheres meanwhile the DME-yield falling was greater (28%) for the regenerated Al-MCM-41 nanospheres. The decrease of the catalytic activity could be due to the carbonaceous species deposition which could promotes the agglomeration of Al and Si surface ions diminishing the amount of exposed active sites with medium acidity, hindering the adequate diffusion of reactants and products or partially blocking of the active sites over the surface. Further research is necessary to promote the catalytic activity by increase of medium acidic sites by the incorporation of metallic ions or functional groups by the coating with inorganic/organic compounds.

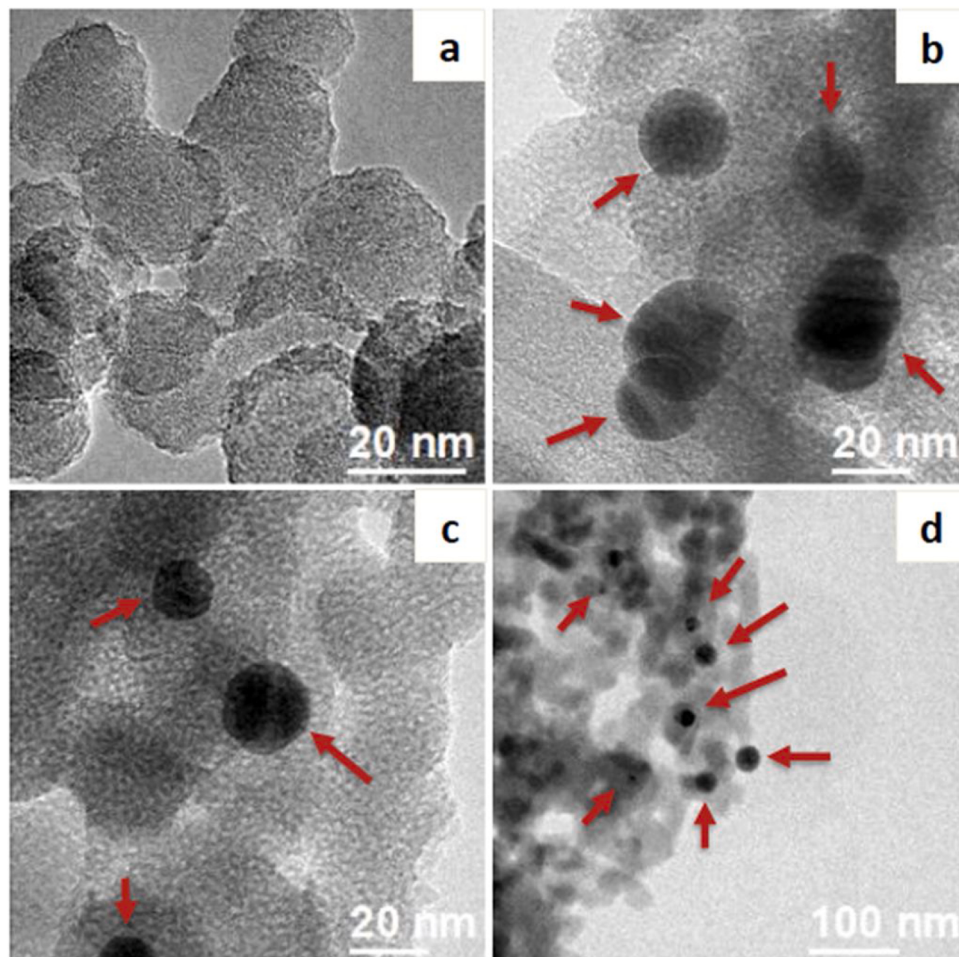


Fig. 9. TEM micrographs of the Al-MCM-41_0.2 nanospheres after 48 h time-on-stream in the methanol dehydration.

Table 3

Summary of the selected mesoporous catalysts used in the synthesis of DME.

Catalyst	T (°C)	P (MPa)	Yield (%)	Stability(h)	Loading (g)	WSHV (h ⁻¹)	Ref.
Al-MCM-41_0.2 nanospheres	300	0.1	78	48	0.2	7.5	This work
Al-MCM-41 (Si/Al = 10) Bulk	300	0.1	50	—	0.5	6	[32]
Al-HMS	300	0.1	89	70	0.5	1	[44]
ZSM-5/MCM-41	300	0.1	80	720	1	12	[45]
HZSM-5	300	1	90	—	1	10, 20	[11]
Al ₂ O ₃ nanocrystals	300	0.1	86	24	0.2	5300*	[9]
γ-Al ₂ O ₃ nanocatalyst	375	0.1	80	216	2	20–50	[6]
CuO-Fe ₂ O ₃ /γ-Al ₂ O ₃	290	0.1	70	8	0.15	1.3	[7]

* GHSV (h⁻¹).

Also, the research of mechanisms to prevent or delay the adsorption of the undesirable species over the surface active-sites is an important issue. In general, the development of mesoporous nanostructures like Al-MCM-41 nanospheres to catalyze the methanol dehydration shows a promising alternative to improving the production of dimethyl ether.

CRediT authorship contribution statement

J.C. Bedoya: Methodology, Investigation, Writing - original draft, Validation, Formal analysis. **R. Valdez:** Investigation, Writing - original draft. **L. Cota:** Validation, Visualization. **M.A. Alvarez-Amparán:** Investigation, Writing - original draft, Validation, Formal analysis, Writing - review & editing. **A. Olivas:** Conceptualization, Investigation, Formal analysis, Funding acquisition, Investigation, Methodology, Project administration, Writing - review & editing.

Declaration of competing interest

The authors report no declarations of interest.

Acknowledgments

The authors thank E. Aparicio, F. Ruiz, J. Mendoza, M. Estrada, and D. Domínguez from CNyN-UNAM and Luis Gradilla from CICESE for their technical support for the materials characterization. J.C. Bedoya and M.A. Alvarez-Amparán acknowledges to CONACYT for MSc scholarship and Postdoctoral fellowship, respectively. This research was financed by the IN107220 grant from DGAPA.

References

- [1] T.A. Semelsberger, R.L. Borup, H.L. Greene, *J. Power Sources* 156 (2006) 497–511.
- [2] J. Sun, N. Tsubaki, G. Yang, Y. Yoneyama, *ACS Catal.* 4 (2014) 3346–3356.
- [3] F. Trippe, M. Fröhling, F. Schultmann, R. Stahl, E. Henrich, A. Dalai, *Fuel Process. Technol.* 106 (2013) 577–586.
- [4] D.A. Good, J.S. Francisco, A.K. Jain, D.J. Wuebbles, *J. Geophys. Res. Atmos.* 103 (1998) 28,181–28,186.
- [5] C. Arcoumanis, C. Bae, R. Crookes, E. Kinoshita, *Fuel* 87 (2008) 1014–1030.
- [6] S.Y. Hosseini, Khosravi M.R.K. Nikou, *J. Ind. Eng. Chem.* 20 (2014) 4421–4428.
- [7] M.A. Armenta, R. Valdez, J.M. Quintana, R. Silva-Rodrigo, L. Cota, A. Olivas, *Int. J. Hydrogen Energy* 43 (2018) 6551–6560.
- [8] C. Chiang, K. Lin, *Int. J. Hydrogen Energy* 42 (2017) 23526–23538.
- [9] J. Khom-in, P. Praserthdam, J. Panpranot, O. Mekasuwandumrong, *Catal. Commun.* 9 (2008) 1955–1958.
- [10] S.M. Solymani, N.A.K. Aboul-Gheit, F.M. Tawfik, M. Sadek, H.A. Ahmed, *Egypt. J. Pet.* 22 (2013) 91–99.
- [11] S.D. Kim, T.K. Kim, C. Zhang, G. Kwak, K.W. Jun, *Catal. Letters* 147 (2017) 792–801.
- [12] S. Jiang, J.-S. Hwang, T. Jin, T. Cai, W. Cho, Y.s. Baek, S.-E. Park, *Bull. Korean Chem. Soc.* 25 (2004) 185–189.
- [13] S. Hosseininejad, R.E. Hayes, A. Afacan, *Chem. Eng. Res. Des.* 90 (2012) 825–833.
- [14] J.S. Beck, J.C. Vartuli, W.J. Roth, M.E. Leonowicz, C.T. Kresge, K.D. Schmitt, C.T. W. Chu, D.H. Olson, E.W. Sheppard, S.B. McCullen, J.B. Higgins, J.L. Schlenker, *J. Am. Chem. Soc.* 114 (1992) 10834–10843.
- [15] D. Zhang, R. Wang, X. Yang, *Catal. Commun.* 12 (2011) 399–402.
- [16] N.A. Fellenz, J.F. Bengoa, S.G. Marchetti, A. Gervasini, *Appl. Catal. A-Gen* 435–436 (2012) 187–196.
- [17] J.M. Campos, J.P. Lourenço, A. Fernandes, M.R. Ribeiro, *Catal. Commun.* 10 (2008) 71–73.
- [18] K. Bachari, R. Chebrou, R.M. Guerroudj, M. Lamouchi, *Res. Chem. Intermed.* 38 (2012) 367–381.
- [19] L.F. Correa, E.A. Alarcón, A.L. Villa, *Ing. Y. Compet.* 14 (2012) 185–196.
- [20] J. WeglarSKI, J. Datka, H. He, J. Klinowski, *J. Chem. Soc. Faraday Transit.* 92 (1996) 5161–5164.
- [21] L.Y. Chen, Z. Ping, G.K. Chuah, S. Jaenicke, G. Simon, *Microporous Mesoporous Mater.* 27 (1999) 231–242.
- [22] S. Udayakumar, S. Ajakumar, A. Pandurangan, *Appl. Catal. A* 307 (2006) 245–256.
- [23] R.M. Martín-Aranda, J. Čejka, *Top. Catal.* 53 (2010) 141–153.
- [24] R. Anuradha, M. Palanichamy, V. Murugesan, *J. Mol. Catal. A* 272 (2007) 198–206.
- [25] D.P. Sahoo, D. Rath, B. Nanda, K.M. Parida, *RSC Adv.* 5 (2015) 83707–83724.
- [26] X. Wang, L. Chen, Q. Guo, *Chem. Eng. J.* 260 (2015) 573–581.
- [27] M. Selvaraj, T.G. Lee, *Microporous Mesoporous Mater.* 85 (2005) 39–51.
- [28] K. Li, B. Wang, D. Bolatibieke, D.-H. Nan, Z.-X. Zhang, M.-S. Cui, Q. Lu, *J. Anal. Appl. Pyrolysis* (2020) 104824, <https://doi.org/10.1016/j.jaat.2020.104824>. In Press.
- [29] X. Liu, S. Min, F. Wang, Z. Zhang, *J. Colloid Interface Sci.* 563 (2020) 112–121.
- [30] E. Martínez-Belmonte, J. Aguilar, M. Gutierrez, J.A. Montoya, J.A. De los Reyes, M. Torres, L.F. Chend, *Cat. Today* 212 (2013) 45–51.
- [31] H. Li, S. He, K. Ma, Q. Wu, Q. Jiao, K. Sun, *Appl. Catal. A Gen.* 450 (2013) 152–159.
- [32] Y. Sang, H. Li, M. Zhu, *J. Porous Mater.* 20 (2013) 1509–1518.
- [33] S.P. Naik, V. Bui, T. Ryu, J.D. Miller, W. Zmierczak, *Appl. Catal. A* 381 (2010) 183–190.
- [34] Y. Chen, X. Shi, B. Han, H. Qin, Z. Li, Y. Lu, J. Wang, Y. Kong, *J. Nanosci. Nanotechnol.* 12 (2012) 7239–7249.
- [35] H. Kosslick, G. Lischke, G. Walther, W. Storek, A. Martin, R. Fricke, *Microporous Mesoporous Mater.* 9 (1997) 13–33.
- [36] A. Ratnamala, V. Durgakumari, K. Lalitha, M. Subrahmanyam, *Catal. Commun.* 8 (2007) 267–274.
- [37] M. Hunger, B. Hunger, J. Hoffmann, O. Heitzsch, *J. Therm. Anal.* 36 (1990) 1379–1391.
- [38] H. Kosslick, G. Lischke, B. Parlitz, W. Storek, R. Fricke, *Appl. Catal. A* 184 (1999) 49–60.
- [39] Z. Zhang, Y. Han, R. Wang, S. Qiu, D. Zhao, F.-S. Xiao, *Stud. Surf. Sci. Catal.* 135 (2001) 198.
- [40] Z. Zhang, Y. Han, F.-S. Xiao, S. Qiu, L. Zhu, R. Wang, Y. Yu, Z. Zhang, B. Zou, Y. Wang, H. Sun, D. Zhao, Y. Wei, *J. Am. Chem. Soc.* 123 (2001) 5014–5021.
- [41] P.G. Moses, J.K. Nørskov, *ACS Catal.* 3 (2013) 735–745.
- [42] Q. Wang, G. Ye, C. Zhang, L. Zhu, X. Song, J. Ma, *J. Mater. Sci.* 49 (2014) 3331–3336.
- [43] J. Dedeček, Z. Sobáfk, B. Wichterlová, *Catal. Rev.* 54 (2012) 135–223.
- [44] M.H. Peyrovi, B. Sabour, T. Hamoule, M. Rashidzadeh, *J. Ind. Eng. Chem.* 20 (2014) 222–227.
- [45] H. Xu, J. Wang, Q. Tang, Y. Zheng, H. Li, J. Zhang, *Appl. Catal. A* 413–414 (2012) 36–42.